Chemodynamics in Blue Compact Dwarf galaxies: II Zw 33 and Mrk 600

F. Campuzano-Castro[1,2], G.F. Hägele[1,2], G. Bosch[1,2], V. Firpo[3], M. Cardaci[1,2], D. Muthukrishna[4] &

N. Morrell[5]

[1] *Instituto de Astrofísica de La Plata, CONICET–UNLP, Argentina*
[2] *Facultad de Ciencias Astronómicas y Geofísicas, UNLP, Argentina*
[3] *Gemini Observatory, La Serena, Chile*
[4] *University of Cambridge, Cambridge, United Kingdom*
[5] *Las Campanas Observatory, Carnegie Observatories, La Serena, Chile*

Contact / fedecampu@gmail.com

Resumen / Realizamos un estudio cinemático de cinco regiones de formación estelar pertenecientes a dos galaxias enanas compactas azules: II Zw 33 and Mrk 600, utilizando datos espectroscópicos de alta resolución obtenidos con el espectrógrafo MIKE del telescopio Clay. Los espectros presentan líneas de emisión con perfiles muy complejos revelando multiples componentes Gaussianas. Con el propósito de analizar la cinemática de estas regiones de formación estelar, desarrollamos un programa en Python, basado en el paquete de minimización de mínimos cuadrados no lineal y ajuste de curvas (*LMFit*), y utilizamos un método estadístico, para analizar la bondad de la inclusión de una nueva componente gaussiana en el modelo. Se estimaron las propiedades físicas del gas (densidades y temperaturas electrónicas), abundancias químicas iónicas y totales de diversas especies atómicas y el grado de ionización en cada región de formación estelar.

Abstract / We performed a kinematic study of five star-formation regions belonging to two Blue Compact Dwarf galaxies: II Zw 33 and Mrk 600, using high resolution spectroscopic data obtained with the MIKE spectrograph mounted at the Clay telescope. The spectra present very complex emission-line profiles showing multiple Gaussian components. In order to analyze the kinematics of these star-forming regions we developed a Python code, based on the Non-Linear Least-Square Minimization and Curve-Fitting (*LMFit*) package, and used a statistical method, to analyze the goodness of the inclusion of a new Gaussian in the model. We estimated the physical conditions (electron densities and temperatures), ionic and total chemical abundances of several atomic species and the ionization degree on each star-forming region.

Keywords / HII regions — galaxies: kinematics, abundance — galaxies: dwarf, individual (IIZw33, Mrk600)

1. Introduction

Blue Compact Dwarf galaxies (BCDs) are objects with luminosities dominated by, at least, one intense star forming knot. Their blue color is due to the UV radiation from young and massive stars (Sargent & Searle, 1970). Distinguished by the presence of active star formation, these objects do not show large amounts of dust or heavy elements (see Hunter & Hoffman, 1999 and Cairós et al., 2001). BCDs are gas-rich objects with mass fractions of HI usually larger than 30 % of the total mass, and present a very similar appearance to the giant HII regions detected in massive galaxies (Sargent & Searle, 1970; Terlevich et al., 1991).

BCDs are considered excellent laboratories to study star formation in low metallicity environments, showing chemical abundances in the range of 1/3 to 1/50 $Z_\odot$ (see Kunth & Östlin, 2000).

II Zw 33 and Mrk 600, are BCDs (catalogued by Gil de Paz et al., 2003) with multiple star forming regions (see Fig. 1). In the next sections, we will present the observations and preliminary results of the multiple components analysis.

2. Observations

Five knots with high Hα emission (three in II Zw 33 and two in Mrk 600) were observed using high resolution spectra with the Echelle double arm spectrograph MIKE, mounted at the Clay 6.5-m Telescope (LCO). No binning was applied to the 2k×4k CCD detector, and the effective slit used for II ZW 33 and Mrk 600 was 0.7" and 1" wide, resulting in a spectral resolution of about 8 and 11 $km\,s^{-1}$, respectively. The spectral range covered by the observations was from $\lambda3300$ Å to $\lambda9300$ Å, guaranteeing the simultaneous measurement of the nebular emission lines from [O II]$\lambda\lambda3726$ Å, 3729 Å to [S III]$\lambda9069$ Å at both ends of spectrum.

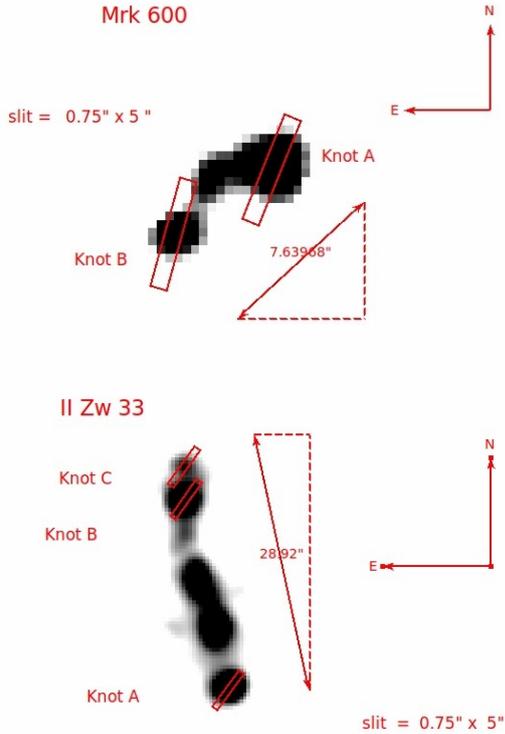The data were reduced using *IRAF* in the usual manner and following the details described in Firpo et al. (2005).

Figure 1: Hα images taken from NED (`https://ned.ipac.caltech.edu/`) with the used slits overimposed

3. Results and discussion

We performed a multiple-Gaussian-components fit to the emission lines in the spectra. To do that we used our own Python code based on *LMFit* function, which provides a high-level interface for non-linear optimization and curve fitting in Python. We used different models combining a linear function (to fit the local continuum) and Gaussian functions (to fit the multiple kinematic components). The parameters to fit are the slope and intercept for the linear function and the velocity, velocity dispersion and amplitude, for the Gaussians.

We used the Akaike indicator to evaluate the statistical relevance of adding a new Gaussian component to the model following Bosch et al. (in preparation). When the addition of such component produces a change in the Akaike Information Criterion ($|\Delta AIC|$) lower than 10 (see Jun-Jie et al., 2016, for details on this criterion), the new component was considered as non statistically significant.

We followed the same methodology as in Hägele et al. (2012) to study the physical conditions estimated for each kinematic component. We assumed a two ionization zone scheme on which the different ions originate (see Garnett, 1992). Depending on their ionization degree:

- High ionization zone: [O III], [Ne III], [Ar IV], He II.
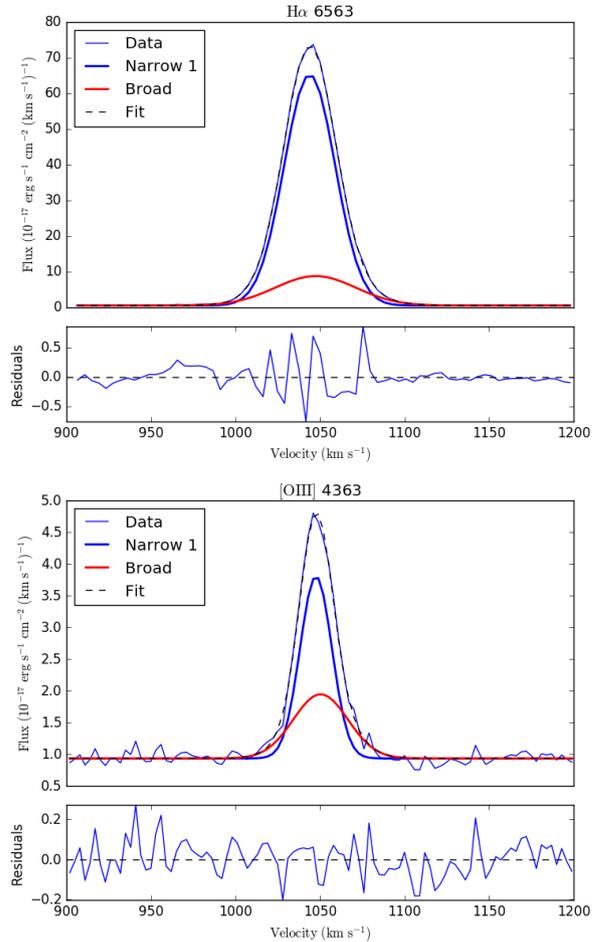- Low ionization zone: H I, [S II], [O II], [O I], [Ar III], [N II].

Figure 2: Multi Gaussian fit to the Hα (upper panel) and the [O III]λ4363 Å auroral emission-line for the knot B of Mrk 600. We over imposed the narrow and broad kinematic components in blue and red, respectively.

The strongest emission-line is the [O III]λ5007 Å for the high ionization, and Hα for the low ionization zone.

For each knot we were able to measure more than twenty emission-lines including some weak auroral emission-lines sensitive to temperature, which are about 1 or 2 % of the [O III]λ5007 Å flux for this kind of objects. In Fig. 2 we show two examples of the fitting performed for the Hα and the [O III]λ4363 Å auroral emission lines, corresponding to the knot B of Mrk 600. Using this kinematic information, we were able to perform a chemodynamic study for the star forming knots, by applying the direct method developed by Hägele et al. (2006, 2008, 2012).

We employed the reddening-corrected, emission-line fluxes to estimate the electron densities (from the [O II]λ3729 Å/3726 Å and [S II]λ6717 Å/6731 Å emission-line ratios) and different electron temperature.

The ionic and total chemical abundances of different species are derived using the strong emission lines present in our spectra, and the adequate electron temperature estimated using (when possible) the direct method, or empirical or theoretical relations. The results for Mrk 600 are in agreement with those
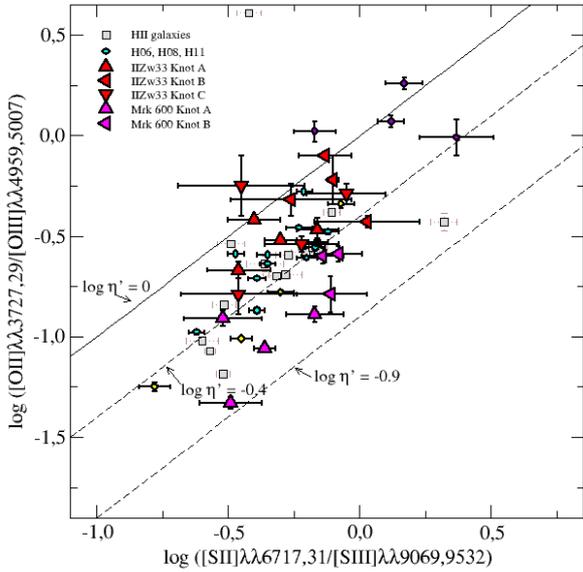
Figure 3: log([O II]/[O III]) vs. log([S II]/[S III]), the η' soft-ness diagram, for the different knots II Zw 33 and Mrk 600 (filled red and violet triangles, respectively), the objects studied in H06, H08 and H11 (turquoise circles), and H II galaxies from the literature as described in H08 (open squares). The diagonals in this diagram correspond to constant values of η'.

estimated by Lagos et al. (2018). With the aim to study the nature of the ionizing sources for the different kinematic components we performed BPT diagnostic diagrams(Baldwin et al. (1981)). In particular we used the [O III]λ5007 Å/Hβ vs.[N II]λ6584/Hα and [O III]λ5007/Hβ vs.[S II]λ(6717+6731) Å/Hα, finding that all the objects and all kinematic components show behaviors compatible with the presence of a star-forming region as the main ionizing source.

We were able to perform an analysis of the ionization structure for the different kinematic components of each star forming knot using the "softness parameter" η ($= (O^+/O^{2+})/(S^+/S^{2+})$), which is intrinsically related to the shape of the ionizing continuum and depends only slightly on the geometry (Vilchez & Pagel, 1988). We were also able to use the pure observational counterpart parameter η'.

$$\eta' = \frac{[\text{O II}]\lambda\lambda 3726, 29 \text{ Å}/[\text{O III}]\lambda\lambda 4959, 5007 \text{ Å}}{[\text{S II}]\lambda\lambda 6717, 31 \text{ Å}/[\text{S III}]\lambda\lambda 9069, 9532 \text{ Å}}.$$

We found different ionization structures for these two galaxies. All the kinematic components of the knots belonging to II Zw 33 are located in a region with lower effective temperatures of the ionizing radiation field, in the η and η' (see Fig. 3) diagrams, than those estimated for the regions belonging to the Mrk 600.

4. Summary

We performed the kinematic decomposition of the emission-line profiles using a Python code developed by us, which is based on the *LMFit* package. We use the Akaike Information Criterion to evaluate the goodness of adding a new Gaussian to the line-profile model. Here we present preliminary results of the first study performed for II Zw 33 and Mrk 600 BCD galaxies.

References

Baldwin J.A., Phillips M., Terlevich R., 1981, A&A, 93, 5
Cairós L.M., et al., 2001, ApJS, 136, 393
Firpo V., Bosch G., Morrell N., 2005, MNRAS, 356, 1357
Garnett D.R., 1992, AJ, 103, 1330
Gil de Paz A., Madore B.F., Pevunova O., 2003, VizieR Online Data Catalog, 214, 70029
Hägele G.F., et al., 2006, MNRAS, 372, 293
Hägele G.F., et al., 2008, MNRAS, 383, 209
Hägele G.F., et al., 2012, MNRAS, 422, 3475
Hunter D.A., Hoffman L., 1999, AJ, 117, 2789
Jun-Jie W., Xue-Feng W., Fulvio M., 2016, A&AS, 90, 285
Kunth D., Östlin G., 2000, ApJS, 10, 1
Lagos P., et al., 2018, MNRAS, 477, 492
Sargent W.L.W., Searle L., 1970, ApJL, 162, L155
Terlevich R., et al., 1991, ApJL, 91, 285
Vilchez J.M., Pagel B.E.J., 1988, MNRAS, 231, 257